Somatomotor and oculomotor inferior olivary neurons have distinct electrophysiological phenotypes

Francisco J. Urbano, John I. Simpson, and Rodolfo R. Llinás*

Department of Physiology and Neuroscience, New York University School of Medicine, 550 First Avenue, New York, NY 10016

The electrophysiological properties of rat inferior olive (IO) neurons in the dorsal cap of Kooy (DCK) and the adjacent ventrolateral outgrowth (VLO) were compared with those of IO neurons in the principal olive (PO). Whereas DCK/VLO neurons are involved in eye movement control via their climbing fiber projection to the cerebellar flocculus, PO neurons control limb and digit movements via their climbing fiber projection to the lateral cerebellar hemisphere. *In vitro* patch recordings from DCK/VLO neurons revealed that low threshold calcium currents, Ih currents, and subthreshold oscillations are lacking in this subset of IO neurons. The recordings of activity in DCK neurons obtained by using voltage-sensitive dye imaging showed that activity is not limited to a single neuron, but rather that clusters of DCK neurons can be active in unison. These electrophysiological results show that the DCK/VLO neurons have unique properties that set them apart from the neurons in the PO nucleus. This finding indicates that motor control, from the perspective of the olivocerebellar system, is fundamentally different for the oculomotor and the somatomotor systems.

oscillations | tremor | eye movement | flocculus

The role of the olivo-cerebellar system in motor control has been the subject of extensive research and much discussion (e.g., refs. 1–3). From the motor perspective the olivocerebellar system has been viewed as involved either in motor learning (e.g., refs. 4–6) or in the timing of motor execution (e.g., refs. 7–9), although some investigators have proposed that these two functions are not mutually exclusive. One of the arguments often voiced against the timing hypothesis is that physiological tremor (8–12 Hz) is present in the somatomotor system (e.g., refs. 10 and 11) but is usually absent in the oculomotor system (e.g., refs. 12 and 13). Physiological tremor in the somatomotor systems has been shown to reflect an important role of electrotonic coupling in the inferior olive (IO) in motor binding and the coherent activation of motoneuron pools responsible for motor execution (8, 14). Physiological tremor is conspicuously absent during the eyes' smooth pursuit of an unpredictably moving object, as well as during ocular fixation (e.g., ref. 13) although microtremors with a frequency near 80 Hz are present (e.g., ref. 15).

In an attempt to comprehend what lies behind the presence or absence of physiological tremor, we compared the electrophysiological properties of IO neurons in the dorsal cap of Kooy (DCK) and the adjacent ventrolateral outgrowth (VLO) with those of IO neurons in the principal olive (PO). DCK/VLO neurons are involved in the control of eye movements via their climbing fiber projection to the cerebellar flocculus, whereas PO neurons are involved in the control of limb and digit movements via their climbing fiber projection to the lateral part of the cerebellar hemisphere (reviewed in refs. 16 and 17).

Here we report a finding that, we believe, goes a long way toward explaining the differences between somatomotor and oculomotor cerebellar control. We found that there is a set of fundamental electrophysiological differences between DCK/VLO neurons and PO neurons. The DCK/VLO neurons lack both T-type calcium channels (18) and the hyperpolarization-activated cationic current (19), known as the Ih current (20, 21), that together are responsible for the intrinsic subthreshold oscillations characteristic of other IO neurons. Recognition of this fundamental difference contributes to resolving contentions in the field of cerebellar motor control. More importantly, the difference between DCK/VLO neurons and PO neurons gives further support to the time binding proposal for the IO contribution to nonoculomotor motricity (7).

Results

Our goal in this study was to determine the electrophysiological and morphological characteristics of the neurons in the DCK/VLO. We compared these characteristics with those of PO neurons, which were usually recorded in the same slice. The PO neuronal results agree with previous electrophysiological findings (19–24).

DCK and VLO nuclei were identified by using the shape of the fourth ventricle and the cerebellar cortical lobules in transverse brain slices (Fig. 1 *A* and *B*). Two dorsal areas corresponding to the prepositus hypoglossi nuclei, as well as the dorsal accessory olive and PO lamellar folds, were also distinctive in our slices. Fig. 1*C* illustrates the morphological differences between biocytin-filled neurons from the DCK and those from the PO. DCK neurons presented a bipolar-like structure with two long, thick dendritic prolongations from the soma, whereas PO neurons presented a spheroidal shape with fine dendrites extending radially in all directions.

DCK neurons recorded in current clamp mode by using a high-potassium intracellular solution responded to the injection of current pulses in a very different way from PO neurons (Fig. 1*D*). In eight instances, both a DCK neuron and a PO neuron were recorded in the same slice. The average input resistance was 43 ± 5 MΩ for DCK (*n* = 14) and 18 ± 2 MΩ for PO (*n* = 10) neurons. Although DCK neurons had larger input resistances than PO neurons (*P* < 0.001), DCK neurons did not show an Ih-current-dependent "depolarizing sag" during hyperpolarization, in contrast to PO neurons (19–23). A T-current-dependent rebound of membrane potential was not observed in DCK neurons at the end of hyperpolarizing pulses, in contrast to PO neurons (19–23). Spontaneous postsynaptic potentials (putative inhibitory postsynaptic potentials; see Fig. 5) were also observed in DCK neurons but not in PO neurons (Fig. 1*D Left*, arrow). When depolarized, DCK neurons responded with a much higher spike frequency than PO neurons (Fig. 1*D*). Indeed, the average spike frequency in DCK neurons could reach 35 Hz, whereas PO neurons only reached 10 Hz (Fig. 1*E*). Interestingly, the electrophysiological and morphological characteristics of DCK neurons were also observed in four additional neurons in the adjacent VLO subnucleus.
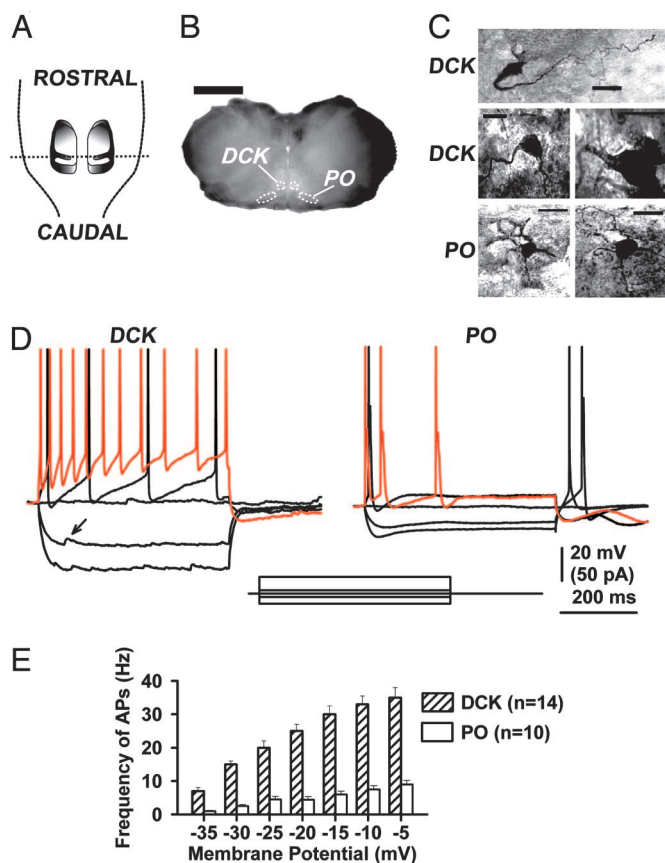
Fig. 1. Basic morphological and electrophysiological properties of DCK and PO neurons. (*A*) Schematic representation of the disposition of the bilateral IO nuclei as observed from the dorsal aspect of the brainstem with the cerebellum removed. (*B*) A fixed 250-μm transverse slice from a 17-day-old rat from the level represented by the dotted line in *A*. DCK and PO areas are outlined schematically with white dots. (Calibration, 2 mm.) (*C*) Biocytin-filled DCK neurons (three examples) and PO neurons (two examples). Each neuron was obtained from a different rat. (Calibration, 20 μm.) (*D*) Responses of a DCK neuron and a PO neuron to square current pulses. Patch recordings (whole-cell current clamp configuration with a high-potassium intracellular solution) show the responses to 500-ms square current pulses of -20, -5, 0, 5, and 30 pA. The response to the 30pA pulse is shown in red. The same differences in response were observed in 14 DCK neurons and 10 PO neurons. Note the presence of spontaneous putative inhibitory postsynaptic potentials in the DCK neuron at hyperpolarizing membrane potentials (arrow in *Left*). (*E*) Average firing frequency (mean ± SEM) of action potentials (APs) in DCK and PO neurons as a function of membrane potential. For each current pulse, the membrane potential was taken as the voltage level just prior to the first action potential. Note that DCK neurons (hatched bars) discharged up to 35 Hz, whereas PO neurons (open bars) only reached 10 Hz.

In addition, although spontaneous subthreshold sinusoidal membrane potential oscillations at 5–10 Hz were described in PO neurons *in vitro* (24), no such subthreshold oscillations were observed in DCK neurons. In fact, DCK neurons had a quite different spontaneous electrical behavior, presenting repetitive-action potentials each followed by a long-lasting afterhyperpolarization, as illustrated in Fig. 2*A*. Moreover, in agreement with previous publications (21, 24, 25), PO neuron membrane polarization modified oscillatory amplitude but not oscillatory frequency. Thus, on average, the frequency of oscillation of PO neurons was not significantly changed with membrane potential (5.8 ± 0.9 at -70 mV to 5.0 ± 0.4 Hz at -40 mV; $n = 12$, $P > 0.05$) (Fig. 2*C*). This electrical property is in contrast with that of DCK neurons, where changes in membrane potential resulted in a linear increase in spike frequency (Fig. 2*C*). The average
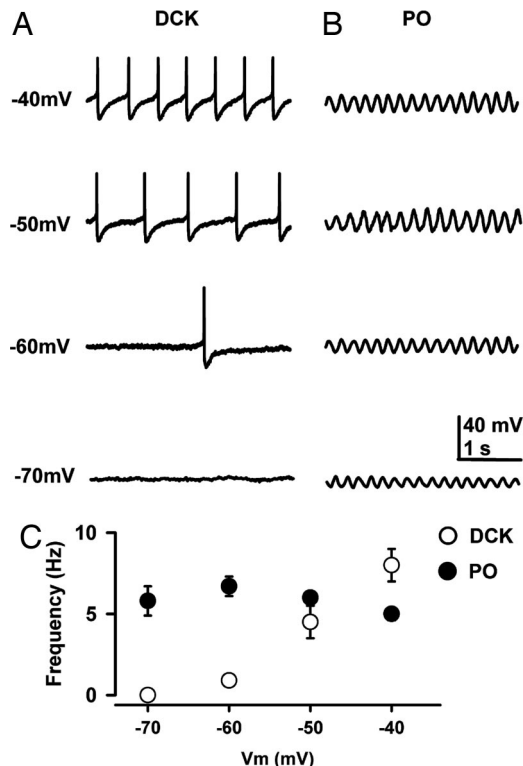

Fig. 2. Repetitive firing of DCK neurons depends on the membrane potential. (*A*) Representative recordings with a high-potassium intracellular solution in the current clamp configuration showing the discharges of a DCK neuron at membrane potentials of -70, -60, -50, and -40 mV. Note that the firing frequency increased with depolarization. Each individual action potential was followed by a large, long-lasting afterhyperpolarization. Action potentials in this figure were truncated to illustrate the afterhyperpolarization amplitude and time course. (*B*) Representative patch recordings from a PO neuron showing subthreshold oscillations at the same membrane potentials as in *A*. Note that the oscillation frequency (5 Hz) hardly changed with membrane potential, although the amplitude changed. The DCK neuron in *A* and the PO neuron in *B* were recorded in the same slice. (*C*) Mean firing frequency (±SEM) of DCK neurons ($n = 11$) and mean frequency (±SEM) of subthreshold oscillations of PO neurons ($n = 10$) as a function of membrane potential. The membrane potentials are the steady-state values reached after injection of a slowly depolarizing ramp current. Note that the frequency of DCK neurons (open circles) increased linearly with membrane potential whereas the frequency of PO subthreshold oscillations (filled circles) remained near 5–7 Hz.

frequency changed from 0 Hz at -70 mV to 8 ± 1 Hz at -40 mV ($n = 11$, $P < 0.05$).

To determine the ensemble dynamics of DCK neuronal activity, we stained transverse slices with the voltage-sensitive dye di-4-ANEPPS (Molecular Probes, Carlsbad, CA) and used a bipolar electrode to deliver 200-μs-wide stimulating pulses at 50 Hz to the edge of the DCK nucleus (Fig. 3; $t = 0$). Following this stimulation, DCK neurons demonstrated time coherent activation (Fig. 3). Thus, both patch and imaging recordings support the idea that the whole DCK can be activated simultaneously.

In DCK neurons, depolarizing square pulses activated a strong outward current at rather negative membrane potentials (about -40 mV; Fig. 4*A*). However, PO neurons presented a very different activation pattern with inward currents followed by a small outward current (Fig. 4*A*). Indeed, using a slow 100-ms voltage ramp (-50–20 mV), we found that the *I–V* curves generated by DCK and PO neurons were clearly different (Fig. 4*B*). Outward currents occurred at more negative potentials in DCK neurons, probably because of a more prominent in-
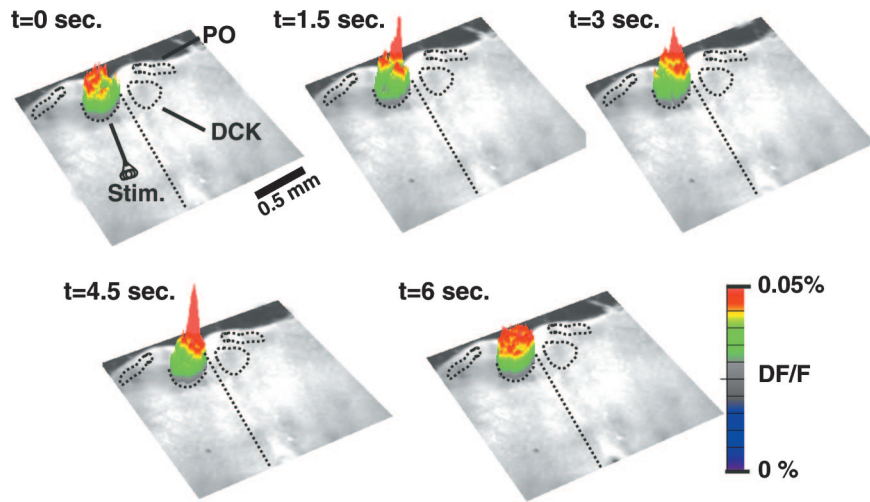
Fig. 3. Voltage-sensitive dye imaging showed ensemble activation of the DCK nucleus. Shown is a sequence of three-dimensional images of the spatiotemporal in fluorescence of a transverse slice stained with the voltage-sensitive dye di-4ANEPPS. The images are superimposed on a contrast photo of the slice. A bipolar electrode delivered a pair of stimuli (two shocks at 200-μs width delivered at 50 Hz) at the edge of the DCK ($t = 0$). Each image represents an average of four consecutive frames taken at a 100-Hz sampling frequency. The baseline activity is represented by the images at $t = 0$ and 6.0 s. The images at $t = 1.5$, 3.0, and 4.5 s show ensemble activation of the DCK nucleus. The locations of the DCK and PO nuclei are also indicated schematically by black dotted lines.

ward current inactivation than in PO neurons. The presence of such a prominent outward current is congruent with the large afterhyperpolarization described above in DCK neurons (see Fig. 2A).

A 100-ms ramp protocol combined with a modified high-cesium (CsMeSO$_3$ + QX-314) intracellular solution was used to compare the subtypes of calcium channels present in DCK and PO neurons. Although DCK neurons showed a single inward peak near −20 mV (Fig. 4C), PO neurons showed two inward components peaking near −20 and −10 mV (Fig. 4D). The same behavior was observed when 100-ms depolarizing square pulses were used. It was further demonstrated, by application of ω-Agatoxin-TK (2 μM; a P/Q-type calcium channel-specific blocker) and ω-Conotoxin-GVIA (10 μM, an N-type calcium channel-specific blocker), that the inward calcium current of DCK neurons was mediated by P/Q-type channels, in contrast to the combination of P/Q- and N-type channels present in PO neurons. The same results were obtained from five DCK neurons and six PO neurons. No blocking effect was observed after the application of ω-Conotoxin-GVIA to DCK neurons ($n = 5$).

DCK neurons are uniquely innervated by a GABAergic input from both the ipsilateral and contralateral prepositus hypoglossi nuclei (26–28) rather than from the cerebellar nuclei. Thus, the presence of inhibition after activation of the prepositus hypoglossi nuclei further identifies these elements as DCK neurons. A high-cesium intracellular solution was used in whole-cell patch clamp mode to demonstrate the equilibrium potential for the inhibitory synaptic events without affecting the inhibitory postsynaptic current (IPSC) battery. Under control conditions with a −80-mV holding potential, an inward current was observed after single shock stimulation near the midline 1 mm from the DCK (Fig. 5A). As expected for a GABA-A-mediated postsynaptic currents (i.e., IPSCs), the polarity of the current gradually reversed in sign as the holding potential was made more positive. Indeed, the *I–V* curve in Fig. 5B for the same cell as in Fig. 5A was nearly linear, with a reversal potential of −21 mV. In addition, the currents were sensitive to picrotoxin, indicating that they were mediated by GABA-A postsynaptic receptors. This result was observed in five DCK neurons and substantiated their identification.

Discussion

The unambiguous results from both the anatomical and electrophysiological characterization of the IO neurons in the DCK/VLO nucleus indicate that they have unique properties that set them apart from the neurons in the PO nucleus. This finding indicates that motor control, from the perspective of the olivo-cerebellar system, is fundamentally different for the oculomotor and the somatomotor systems.

Anatomical Characteristics. Intracellularly labeled biocytin-filled DCK neurons ($n = 14$) had dendrites that were organized in a bipolar-like arrangement that extended farther from the soma than the spherically bounded dendritic arbor of PO neurons ($n = 10$). Although previous studies have shown that IO neurons have these two distinctive morphologies (29–31), the fact that only one of them is present in the DCK/VLO was not previously recognized.

Electrophysiological Properties: Voltage Recordings. *In vitro* patch recordings from DCK/VLO neurons revealed that, in marked contrast to the now classical findings for all other previously studied IO neurons, low-threshold calcium currents, Ih currents, and subthreshold oscillations are lacking in this subset of IO neurons. More specifically, as shown in Fig. 1, current clamp recordings from DCK neurons show that these cells lack both activation of low-threshold calcium spikes from a negative resting membrane potential and the characteristic rebound response observed in PO neurons after hyperpolarization from the resting potential. Moreover, the rectification due to Ih activation is also lacking (Fig. 1). The difference in subthreshold oscillation between DCK and PO neuron is also striking. Whereas PO neurons show a clear subthreshold oscillation whose frequency is nearly insensitive to membrane potential, DCK neurons show no such oscillation (Fig. 2). When DCK neurons are depolarized they do not fire at high frequency in comparison with most other CNS neurons; however, with substantial depolarization, they can attain spike frequencies beyond 30 Hz despite the strong afterhyperpolarization. In contrast, PO neurons have a more prominent afterhyperpolarization that prevents firing frequencies above 10 Hz (Fig. 1). The difference in the electrical behavior of these two types of IO neurons is that

Fig. 4. DCK neurons presented a different pattern of outward potassium and inward calcium currents than PO neurons. (*A*) Representative currents in DCK and PO neurons in response to 100-ms depolarizing square pulses recorded by using a high-potassium electrode solution. Note that in PO neurons, inward currents were followed by a small outward current. In DCK neurons, the same depolarizing square pulses activated a strong outward current. The holding potential was −60 mV in both cases. (*B*) I–V curve generated by using a 100-ms ramp of voltage from −50 to 20 mV for the same cells as in *A*. (*C* and *D*) With a modified high-cesium (CsMeSO$_3$ + QX-314) electrode solution, the same ramp protocol used in *B* was able to elicit only inward calcium currents. Although DCK neurons presented a single peak around −20 mV (*C*), two inward components, peaking around −20 and −10 mV, were observed for PO neurons (*D*). The use of specific toxins (2 μM ω-Agatoxin-TK and 10 μM ω-Conotoxin-GVIA, which are P/Q- and N-type specific blockers, respectively) demonstrated that the inward calcium currents of DCK neurons were mediated only by P/Q-type channels, in contrast to the combination of P/Q- and N-type channels present in PO neurons. The same results were obtained from five DCK neurons with ω-Agatoxin-TK and six PO neurons with both ω-Agatoxin-TK and ω-Conotoxin-GVIA. No blocking effect was observed after the application of ω-Conotoxin-GVIA to DCK neurons (*n* = 5).

with increasing depolarization, DCK neurons increase their firing to frequencies much higher (35 Hz) than the 10 Hz upper limit of PO neurons. Also, although DCK/VLO neurons can occasionally show weak rhythmic activity in the 6- to 12-Hz range in response to their excitatory afferent input that signals retinal image movement (32, 33), PO neurons are characterized by robust rhythmicity at 6–12 Hz (9).

Electrophysiological Properties: Ionic Current Recordings. Patch clamp experiments revealed that the marked differences in activity between PO and DCK neurons (Figs. 1 and 2) are determined by the differences in their ionic conductances (Fig. 4). Thus, as previously demonstrated, PO neurons have a low-threshold calcium current (reviewed in ref. 18) that is supported by T-type calcium channels (Ca$_V$3.1) and is blocked by octanol (34) and a high-threshold calcium current that is carried by P/Q- and N-type calcium channels (Ca$_V$2.1 and Ca$_V$2.2) (22–24, 35, 36). In contrast, DCK neurons have only one voltage-dependent calcium current, which is completely blocked by ω-Agatoxin-TK, indicating that it is supported by P/Q-type calcium channels.

Voltage-Sensitive Dye Imaging. The recordings of activity in DCK neurons obtained by using voltage-sensitive dye imaging (Fig. 3) showed that activity is not limited to a single neuron but rather that clusters of DCK neurons can fire in unison. This finding

Fig. 5. DCK neurons are innervated by GABAergic terminals. Voltage clamp experiments were conducted by using a high-cesium (CsMeSO$_3$ + QX-314) electrode solution in combination with single-shock stimulation of afferents to the DCK from the prepositus hypoglossi nuclei. (*A*) Representative examples of IPSCs at five membrane holding potentials (−80, −60, −40, −20, and 0 mV). The same result was observed in 5 DCK neurons. The IPSCs were mediated by a GABA-A receptor because a local application of picrotoxin (100 μM) blocked them reversibly (*n* = 5). Because DCK neurons have a GABAergic connectivity not shared by other IO neurons, the inhibitory input described here is a critical additional marker. The data shown in *A* are plotted in *B* as the I–V curve of IPSC amplitude versus the holding potential. The reversal potential was −21 mV. (*C*) Schematic drawing indicating the climbing fiber projection (in red) of DCK neurons to the contralateral cerebellar flocculus, and the afferent GABAergic input (in green) to the DCK from the bilateral prepositus hypoglossi nuclei. Fl, flocculus; Pfl, paraflocculus; PHN, prepositus hypoglossi nuclei.

strongly implies that, as in the case of PO neurons, DCK neurons are electrically coupled and thus can fire close to isochronally, as reported for *in vivo* experiments (32, 37).

Thoughts About Functional Significance. The striking differences between DCK/VLO neurons and PO neurons in both their electrophysiology and morphology clearly imply that parts of the IO nucleus operate in at least two different modes. These differences, considered together with the difference in the cerebellar projection of DCK/VLO neurons (Fig. 5*C*) and PO neurons, agree with the absence of physiological tremor in the oculomotor system and its presence in the somatomotor system. Even so, the findings reported here demand some hypothesis that addresses the necessity of two types of IO neurons in the organization of coordinated motricity. Whereas the importance of a timing signal has been theoretically assigned to the requirements of temporal binding (e.g., refs. 7, 10, and 11) to allow time coherence of motoneuron activation to serve as the element basic to somatomotor coordination, a similar case may also be made for the oculomotor system. So what would be the difference between somatic and ocular motricity that would require such a dramatic functional differentiation? One hypothesis relates to the multiple-joint organization of the somatomotor system, as opposed to the single-joint organization of the ocu-

lomotor system. In the former case, multiple parameters corresponding to different coordinate systems must operate in unison to attain coordination. The tremendous complexity afforded by such a massive coactivation of motoneuron pools means that the temporal requirements become astronomically complex. To this requirement is added muscle feedback that operates in all myotatic reflexes, in which muscle spindles are simultaneously informing the CNS about position and rate of movement for each of the segments of multijointed limbs. Therefore, a simplifying control approach seems to be required to restrict movement to the effector feedback properties that characterize somatomotor movements. In contrast, oculomotor activity does not require such a computationally complex approach to motor generation, because the task requires regulating only one vector in three-dimensional space (e.g., refs. 12 and 38), but with a degree of precision not usually demanded of the somatomotor system. Indeed, eye movement fixation in humans is modulated by the microsaccadic system, which operates at $\approx 0.2°$ of amplitude at a frequency of 1–2 Hz (e.g., refs. 12 and 39). The somatomotor system requires a less precise range of amplitude control, but it must operate under conditions where the movement load and momentum vary continuously as, for example, when objects are reached for, held, and lifted. In short, we may consider the differences in motor control requirements between somatic and ocular motricity as the evolutionary pressure that ultimately led to the dramatic differences in the electrophysiological properties of DCK/VLO neurons and PO neurons.

Materials and Methods

Obtaining Slices Containing the DCK. Animal usage and experiment methods were approved by the Institutional Animal Care and Use Committee of the New York University School of Medicine. Thirty-two rats were used for whole-cell patch recordings in conjunction with ultrafast voltage-sensitive dye imaging. Two- to three-week-old Long–Evans rats (40–50 g, either sex; Taconic Farms, Hudson, NY) were anesthetized with pentobarbital (Nembutal, 120 mg/kg i.p.; Abbott Laboratories, North Chicago, IL) and decapitated. The bone and dura covering the cortical surface were carefully peeled away. The rostral part of the brain was glued to the stage of a Leica vibroslicer (Leica, Bannockburn, IL) and submerged in a chamber containing a chilled low-Na^+/ACSF (high-sucrose artificial cerebrospinal fluid) solution [248 mM sucrose/26 mM $NaHCO_3$/1.25 mM NaH_2PO_4/5 mM KCl/3 mM $MgSO_4$/0.5 mM $CaCl_2$/10 mM (+)-sodium-L-ascorbate/3 mM sodium pyruvate/10 mM glucose, aerated with 95% O_2 and 5% CO_2 to a pH of 7.4]. Transverse slices (250–300 μm thick) were obtained between the spinal cord and the rostral part of the cerebellar cortex (Figs. 1 *A* and *B*). The topographical organization of the IO has been extensively described in the rat as comprising three major nuclei: (*i*) the medial accessory olive, the dorsal accessory olive, and the PO (40–42). The small subnuclei (DCK) and the adjacent VLO are included in the medial accessory olive (41). Three to four slices containing different portions of the DCK, as well as the VLO, were usually obtained. The PO was also included in the same slices. The slices were allowed to recover in an incubation chamber at 37°C for at least 30 min. The chamber contained a continuously oxygenated combination of 50% low-Na^+/high-sucrose (see above) and 50% normal high-sucrose artificial cerebrospinal fluid solution (124 mM NaCl/5 mM KCl/1.25 mM KH$_2$PO4/26 mM $NaHCO_3$/1.2 mM $MgCl_2$/2.4 mM $CaCl_2$/10 mM glucose, pH 7.4).

Whole-Cell Patch Recordings. Patch recordings were made at 35°C in an interphase chamber perfused with normal high-sucrose artificial cerebrospinal fluid solution. Patch electrodes were made from borosilicate glass and had resistances of 3–8 MΩ when filled with either a high-potassium intracellular solution (130 mM KMeSO$_3$/10 mM NaCl/10 mM Hepes/1 mM EGTA/4 mM Mg-ATP/0.4 mM Na-GTP/2 mM $MgCl_2$/10 mM sucrose/10 mM phosphocreatine, pH 7.3, 290 mOsm) or a high-cesium/QX314 intracellular solution (120 mM CsMeSO$_3$/8 mM NaCl/10 mM Hepes/5 mM EGTA/10 mM TEA-Cl/4 mM Mg-ATP/0.5 mM GTP/7 mM phosphocreatine, pH 7.3, 290 mOsm). Prior to patch recordings being performed, 2 mg/ml biocytin was included in the intracellular solution to permit characterization of the recorded neuron's morphology. Neurons were recorded by using an Axopatch 200A amplifier (Molecular Devices, Sunnyvale, CA) in combination with PCLAMP 10.0 software (Molecular Devices). Data were filtered at 5 kHz, digitized, and stored for off-line analysis. Access resistance (8–25 MΩ) was continuously monitored during the experiments. Bipolar electrical stimulation (twice threshold), close to the midline and 1 mm below the prepositus hypoglossi nuclei, resulted in IPSCs only in DCK neurons.

Voltage-Sensitive Dye Imaging. As described in ref. 43, the voltage-sensitive dye imaging apparatus consisted of a 12-V halogen light source, a filter (515 $\pm$ 35 nm), a dichroic mirror, and a microscope objective (magnification $\times$5). The slice was stained with the voltage-sensitive dye di-4-ANEPPS (absorption, 496 nm; emission, 705 nm). The emitted fluorescent light was lowpass filtered (>590 nm) and imaged by using a charged-coupled device camera (MiCAM ULTIMA; BrainVision, Tokyo, Japan). Images were collected every 10 ms. Paired-pulse stimulation (50 Hz) was delivered close to the DCK nucleus to reset the membrane potential.

Final optical recordings were analyzed by using BrainVison Analyzer software (BrainVision). In brief, the recordings were detrended to compensate for dye bleaching and for slow responses from glia cells (44, 45) and three-dimensionally averaged. Changes in membrane potential were evaluated as DF/F. The optical signals were displayed by using the RGB 256 color scale in such a way that their maximum amplitude equaled the maximum red color intensity of the RGB scale.

Morphological Identification of Neurons. Recorded neurons were identified by using the ABC kit–DAB method after biocytin injection during patch clamp recordings. Slices were fixed overnight by using a 4% paraformaldehyde solution in 0.1 M PBS (pH 7.4) at 4°C, washed three times in 0.1 M PBS for a total of 30 min, and further incubated in a 0.1% solution of Triton X-100 in 0.1 M PBS. The slices were then transferred to an VECTASTAIN ABC solution (Peroxidase Standard PK-400 kit; Vector Laboratories, Burlingame, CA), dehydrated, and mounted.

Pharmacological Reagents. Drugs were applied by pressure locally through a pipette. Drugs were purchased from Sigma-Aldrich (St. Louis, MO). The voltage-sensitive dye di-4-ANEPPS was purchased from Molecular Probes.

1. Simpson JI, Wylie DR, De Zeeuw CI (1996) *Behav Brain Sci* 19:384–398.
2. Llinás R, Leznik E, Makarenko V (2002) *Ann NY Acad Sci* 978:258–272.
3. Gibson AR, Horn KM, Pong M (2004) *Cerebellum* 3:212–221.
4. Ito M (2001) *Physiol Rev* 81:1143–1195.
5. Hesslow G, Yeo CH (2002) in *A Neuroscientist's Guide to Classical Conditioning*, ed Moore JW (Springer, Berlin), pp 86–146.
6. Highstein SM, Porrill J, Dean P (2005) *Cerebellum* 4:140–150.
7. Llinás RR (1991) in *Motor Control: Concepts and Issues*, eds Humphrey DR, Freund H-J, (Wiley, London), pp 223–242.
8. Welsh JP, Lang EJ, Sugihara I, Llinás R (1995) *Nature* 374:453–454.
9. Lang EJ, Sugihara I, Welsh JP, Llinás R (1999) *J Neurosci* 19:2728–2739.
10. Vallbo B, Wessberg J (1993) *J Physiol (London)* 469:673–691.

11. Farmer SF (1998) *J Physiol (London)* 509:3–14.
12. Carpenter RHS (1977) *Movements of the Eyes* (Pion, London).
13. McAuley JH, Rothwell JC, Marsden CD (1999) *Neuroscience* 94:339–350.
14. Placantonakis DG, Bukovsky AA, Zeng XH, Kiem HP, Welsh JP (2004) *Proc Natl Acad Sci USA* 101:7164–7169.
15. Bolger C, Bojanic S, Sheahan NF, Coakley D, Malone JF (1999) *Vision Res* 39:1911–1915.
16. Voogd J, Bigaré F (1980) in *The Inferior Olivary Nucleus: Anatomy and Physiology*, eds Courville J, de Montigny C, Lamarre Y (Raven, New York), pp 207–234.
17. Ito M (1984) *The Cerebellum and Motor Control* (Raven, New York).
18. Llinás R (1988) *Science* 242:1654–1664.
19. Yarom Y, Llinás R (1987) *J Neurosci* 7:1166–1177.
20. Bal T, McCormick DA (1997) *J Neurophysiol* 77:3145–3156.
21. Long MA, Deans MR, Paul DL, Connors BW (2002) *J Neurosci* 22:10898–10905.
22. Llinás R, Yarom Y (1981) *J Physiol (London)* 315:549–567.
23. Llinás R, Yarom Y (1981) *J Physiol (London)* 315:569–584.
24. Llinás R, Yarom Y (1986) *J Physiol (London)* 376:163–182.
25. Leznik E, Llinás R (2005) *J Neurophysiol* 94:2447–2456.
26. Barmack NH, Fagerson M, Errico P (1993) *J Comp Neurol* 328:263–281.
27. De Zeeuw CI, Wentzel P, Mugnaini E (1993) *J Comp Neurol* 327:63–82.
28. Arts MP, De Zeeuw CI, Lips J, Rosbak E, Simpson JI (2000) *J Neurophysiol* 84:2552–2563.
29. Schiebel ME, Schiebel AB (1955) *J Comp Neurol* 102:77–132.
30. Foster RE, Petersen BE (1986) *Brain Res Bull* 17:785–800.
31. Devor A, Yarom Y (2002) *J Neurophysiol* 87:3048–3058.
32. Wylie DR, De Zeeuw CI, Simpson JI (1995) *J Neurosci* 15:2875–2887.
33. Simpson JI, Wylie DR, De Zeeuw CI (1996) *Behav Brain Sci* 19:496–498.
34. Sinton CM, Krosser BI, Walton KD, Llinás RR (1989) *Eur J Physiol* 414:31–36.
35. Regehr WG, Mintz IM (1994) *Neuron* 12:605–613.
36. Placantonakis DG, Welsh JP (2001) *J Physiol (London)* 534:123–140.
37. De Zeeuw CI, Koekkoek SKE, Wylie DRW, Simpson JI (1997) *J Neurophysiol* 77:1747–1758.
38. Van der Steen J, Simpson JI, Tan J (1994) *J Neurophysiol* 72:31–46.
39. Bridgeman B, Palca J (1980) *Vision Res* 20:813–817.
40. Paxinos G, Watson C (1982) *The Rat Brain in Stereotaxic Coordinates* (Academic, Sydney).
41. Azizi SA, Woodward DJ (1987) *J Comp Neurol* 263:467–484.
42. Ruigrok TJH, Osse RJ, Voogd J (1992) *J Comp Neurol* 316:129–150.
43. Leznik E, Makarenko V, Llinás R (2002) *J Neurosci* 22:2804–2815.
44. Konnerth A, Obaid AL, Salzberg BM (1987) *J Physiol (London)* 393:681–702.
45. Lev-Ram V, Grinvald A (1986) *Proc Natl Acad Sci USA* 83:6651–6655.

NEUROSCIENCE